Multistable Morphing Mechanisms of Nonlinear Springs

Chrysoula Aza[1]
Bristol Composites Institute (ACCIS), Department of Aerospace Engineering, University of Bristol
Bristol, BS8 1TR, UK
e-mail: chrysoula.aza@bristol.ac.uk

Alberto Pirrera
Bristol Composites Institute (ACCIS), Department of Aerospace Engineering, University of Bristol
Bristol, BS8 1TR, UK
e-mail: alberto.pirrera@bristol.ac.uk

Mark Schenk
Bristol Composites Institute (ACCIS), Department of Aerospace Engineering, University of Bristol
Bristol, BS8 1TR, UK
e-mail: m.schenk@bristol.ac.uk

ABSTRACT

Compliant mechanisms find use in numerous applications both in micro and macro scale devices. Most of the current compliant mechanisms base their behavior on beam flexures. Their range of motion is thus limited by the stresses developed upon deflection. Conversely, the proposed mechanism relies on elastically nonlinear components to achieve large deformations. These nonlinear elements are composite morphing double-helical structures that are able to extend and coil like springs, yet, with nonlinear stiffness characteristics. A mechanism consisting of such structures, assembled in a simple truss configuration, is explored. A variety of behaviors is unveiled that could be exploited to expand the design space of current compliant mechanisms. The type of behavior is found to depend on the initial geometry of the structural assembly, the lay-up, and on other characteristics specific of the composite components.

1. Introduction

Compliant devices have been of great interest among researchers in the fields of mechanisms, robotics and morphing structures. The interest stems from their potential and the variety of promising applications both at the micro and macro scale [1]. Mechanisms are parts of machines and other devices used to transfer motion, force or energy. Conventional mechanisms consist of rigid links and base their performance on movable joints. Unlike rigid-link mechanisms, compliant mechanisms utilize the flexibility of their members to transmit or transform motion and forces [2]. The field of application for compliant mechanisms is broad [1]. They can be used in precision positioning systems, *e.g.* optical fiber alignment [3], in rehabilitation devices [4], in MEMS/NEMS such as switchers [5], in nano-injectors [6], deployable structures [7] or space applications [8]. Compliant mechanisms can also be employed for efficient energy harvesting or vibration isolation [9,10].

Compliant mechanism can be considered as springs with variable stiffness. To modulate their stiffness characteristics or to achieve nonlinear behavior, combinations of cam and beam structures [11] or cam rollers with floating springs have been used, leading to complex and relatively bulky designs [12]. State-of-the-art compliant mechanisms take advantage of the flexibility of their constituent materials to obtain designs that are lightweight, easily scalable and with reduced friction and no need for lubricants. However, these compliant mechanisms often rely on flexures, whose range of motion is limited by the stresses developed upon elastic deformation [13]. To achieve higher effective strains and extend the range of motion currently available, this work proposes the use of morphing composite structures as the flexible elements in a compliant mechanism.

Morphing structures are able to change shape and undergo large deformations while maintaining their load-carrying capability and structural integrity [14]. In the present work, the composite double-helical structure proposed by Lachenal *et al.* [14,15] has been selected as the deformable component for compliance. This morphing structure exhibits multistability

[1] Corresponding author.

and nonlinear stiffness characteristics that can be tailored to meet specific desirable behaviors. For simplicity and for the sake of illustration, in this work, the double-helical structures are combined into a simple truss-like compliant mechanism, resembling a *von Mises* truss. The result is a rich mechanical response stemming from the interaction of geometric and elastic nonlinearity, as well as the inherent nonlinearity of the morphing components.

The proposed illustrative mechanism could be used as the structural building block to design more complex assemblies for bespoke mechanical properties and kinematics, *e.g.* [16,17]. For instance, lattice structures have already been shown to be able to provide unique combinations of properties and behaviors [16,18]. In this respect, by tailoring its architecture and properties, the proposed mechanism may be used as the unit cell to create 2D and 3D structures with reconfigurable behavior, for dynamic applications, energy efficiency, to control structural deployability or isolate vibrations [18].

In addition to introducing the said compliant mechanism, the aim of this paper is to demonstrate the richness of its design space and the range of attainable mechanical behaviors. The remainder of the paper is organized as follows. Section 2 presents the analytical model and the nonlinear elastic behavior of the compliant double-helical structure, followed by a description of the analysis and synthesis methods for assemblies of double-helices in a *von Mises*-like truss configuration. Results are presented in section 3 as energy landscapes and equilibrium manifolds. The effect of various design parameters on desirable features, such as multistability and constant stiffness, is explored. A prototype of the new mechanism is manufactured and experimental results are presented in section 4. Finally, concluding remarks are given in section 5.

2. Structural Assemblies of Double-Helices

2.1 Double-Helix Structure

The helical structure (Fig. 1) consists of two prestressed carbon fiber reinforced polymer strips of dimensions $L \times W$ connected by rigid spokes to keep them apart at a constant distance $H = 2R$, where R is the radius of an underlying cylinder upon which the deformed strips are assumed to lie [15,19]. Prestress is introduced by manufacturing the strips on a cylindrical mold of radius R_i and subsequently flattening them, to form the double-helix. The structure can deform continuously from an uncoiled (straight) configuration to coiled configurations defined by the angle $\theta \in [-90°, 90°]$ representing the pitch of the helix. The angle θ is defined to be positive for anti-clockwise rotations starting from the straight configuration (Fig. 1) [14]. The lay-up of the composite strips can be tailored to influence the mechanical response of the double helix. In this work, we focus on helix deformation limited to $\theta \in [0°, 90°]$ and on lay-ups of five plies of the form $[\beta_2/0/\beta_2]$ and $[\beta_2/0/\text{-}\beta_2]$, where β is the fiber angle measured with respect to the local x-axis of the strips. The angle β is defined to be positive towards the y-axis (see Fig. 1a) and the plies are stacked in the positive z-direction. Figure 2 shows a manufactured prototype of the helix.

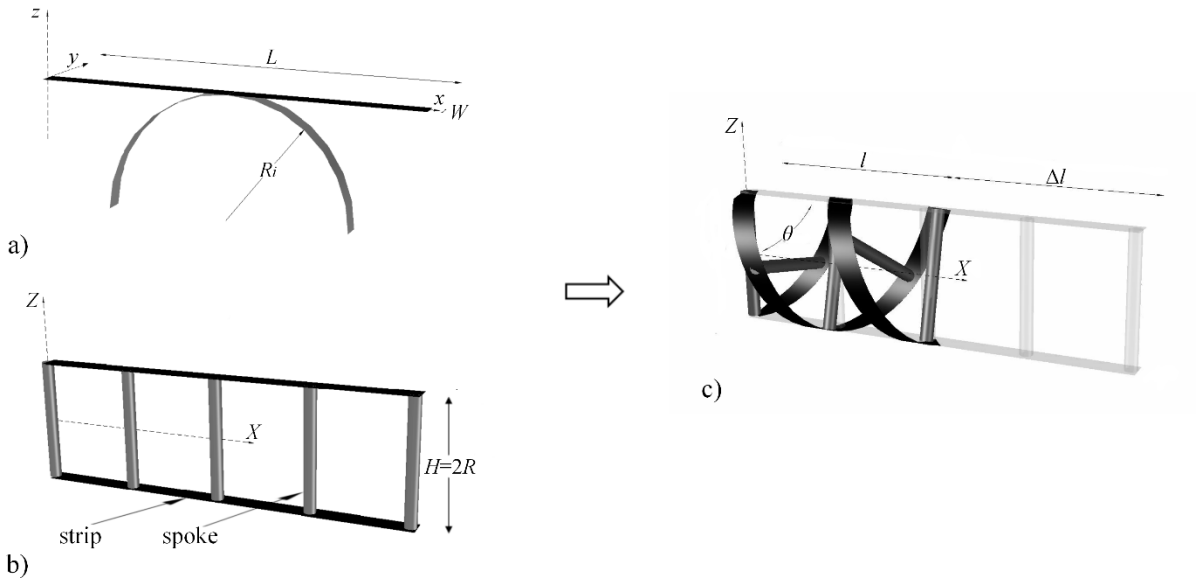

Figure 1: a) Initially curved (radius R_i) composite strips are flattened to introduce prestress; b) the strips are joined by rigid spokes to form a double-helix structure, which c) can deform from a straight (light grey) to a twisted (dark) configuration ($\theta < 0$).

Figure 2: Manufactured prototype of the double-helix structure in a) straight, b) stable twisted, c) unstable twisted and d) fully coiled configuration.

The analytical model of the composite structure [14,15] is based on its total strain energy, calculated as:

$$U = \frac{n}{2}\int_0^L \int_{-W/2}^{W/2} \begin{bmatrix} \boldsymbol{\varepsilon}^0 \\ \Delta\boldsymbol{\kappa} \end{bmatrix}^{\mathrm{T}} \begin{bmatrix} \mathbf{A} & \mathbf{B} \\ \mathbf{B} & \mathbf{D} \end{bmatrix} \begin{bmatrix} \boldsymbol{\varepsilon}^0 \\ \Delta\boldsymbol{\kappa} \end{bmatrix} dydx, \tag{1}$$

where n is the number of composite strips, $\boldsymbol{\varepsilon}^0$ is the mid-plane strain tensor and $\Delta\boldsymbol{\kappa}$ is the tensor of the change in curvature, both referred to the local coordinate system of the strips. **A**, **B** and **D** are the in-plane, bending-extension coupling and bending stiffness matrices from Classical Laminate Theory [20]. Conceptually, a symmetric lay-up, *i.e.* the $[\beta_2/0/\beta_2]$ lay-ups herein, exhibits no coupling between bending and extensional responses, while a balanced and antisymmetric lay-up, *i.e.* the $[\beta_2/0/\text{-}\beta_2]$ lay-ups, exhibits no extension-shear or bend-twist coupling. Following the assumption by Giomi and Mahadevan [21] that only x-axis strains are developed during the deformation of the structure, and noting that the bending-extension contribution can be neglected due to the near-zero B_{11} for the selected composite lay-ups, the strain tensor is calculated as:

$$\boldsymbol{\varepsilon}^0 = \begin{bmatrix} \varepsilon_x^0 \\ \varepsilon_y^0 \\ \gamma_{xy}^0 \end{bmatrix} = \begin{bmatrix} \alpha_{11} N_x \\ 0 \\ 0 \end{bmatrix}, \tag{2}$$

where α_{11} is a term of the compliance matrix **S**:

$$\mathbf{S} = \begin{bmatrix} \mathbf{A} & \mathbf{B} \\ \mathbf{B} & \mathbf{D} \end{bmatrix}^{-1}, \tag{3}$$

and N_x is the axial force arising upon deformation. Further, assuming constant curvatures $\Delta\kappa_x$ and $\Delta\kappa_{xy}$ along the length L and width W of the strip, while letting the transverse curvature $\Delta\kappa_y$ vary along the width, $\Delta\boldsymbol{\kappa}$ becomes:

$$\Delta\boldsymbol{\kappa} = \begin{bmatrix} \Delta\kappa_x \\ \Delta\kappa_y \\ \Delta\kappa_{xy} \end{bmatrix} = \frac{1}{2R}\begin{bmatrix} 1 - \cos(2\theta) - \dfrac{2R}{R_i} \\ 2R\Delta\kappa_y^i \\ 2\sin(2\theta) \end{bmatrix}, \tag{4}$$

where $\Delta\kappa_y^i$ refers to the transverse change of curvature as developed in [14].
The axial force F necessary to extend or contract the helix is derived from the strain energy by applying Castigliano's theorem [15]:

$$F = \frac{\partial U}{\partial \Delta l}, \tag{5}$$

where Δl is the deformation of the structure from the straight configuration.

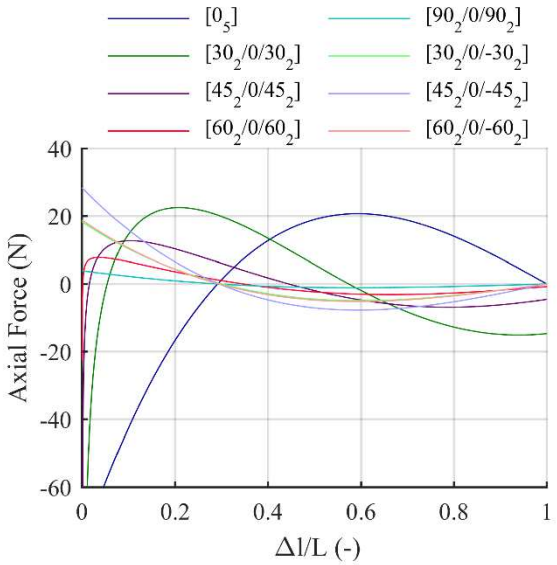

Figure 3: Load-displacement curves of double-helices for different lay-ups of the form [β_2/0/β_2] or [β_2/0/-β_2], where β is the ply angle. The displacement Δl is normalized to the length L of the strips, with $\Delta l/L = 0$ representing the fully-extended and $\Delta l/L = 1$ its fully coiled configuration. All double-helices shown have two self-equilibrated configurations with no external force required to maintain the shape.

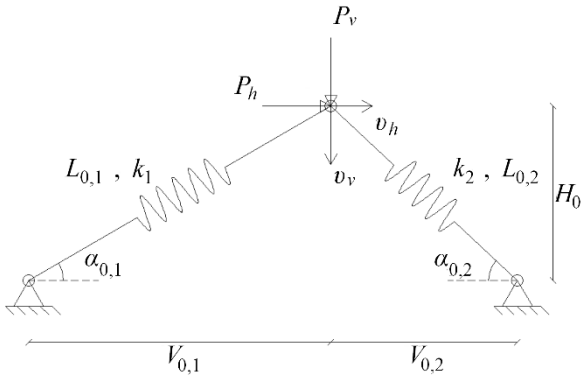

Figure 4: Schematic representation of the assembly of double-helices in a truss-like configuration with both supports pinned [22]. The initial configuration is determined by the equilibrium length $L_{0,i}$ of the double-helices and by the initial angle $\alpha_{0,i}$ of the truss configuration.

Figure 3 shows the axial force versus displacement curves for the double-helices used in this paper (L = 95 mm, R = 15 mm, R_i = 30 mm, W = 5 mm). The response of the double-helix is nonlinear, with both axial force and stiffness changing sign as the helix deforms from the extended ($\Delta l/L = 0$) to the fully coiled ($\Delta l/L = 1$) configuration. All double-helices considered here have multiple configurations of self-equilibrium ($F = 0$), although these are not always stable. The behavior of the double-helix is determined by the dimensions of the structure, the prestress of the strips, and the lay-up of the composite plies [19]. The lay-up of the composite strip affects the stiffness characteristics of the helices through the **A**, **B** and **D** matrices, resulting in different shapes of the load-displacement curves for helices of different lay-ups (see Fig. 3). In comparison, the geometrical features of the helix affect only the magnitudes of the load-displacement curves. In this sense, the lay-up of the composite strips has the most significant effect on the load-displacement curves of the double-helices and is therefore shown here; for brevity, the sensitivity to varying geometric parameters is shown in Appendix A.1.

2.2 Structural Assemblies of Double-Helices

The double-helix can deform from an extended to a completely coiled configuration, and functions as a nonlinear spring. The present work further explores these elements and their nonlinearities, combining them in structural assemblies. The proposed assembly forms a truss-like structure, as shown in Fig. 4. The assembly is a 2-degree-of-freedom, modified *von Mises* truss with two double-helices forming the truss members, connected by pin joints at the apex and base. Consequently, the truss members are only loaded axially. As such, their transverse and bending stiffness characteristics are not considered here. In its initial configuration, the structure has height H_0 and a base angle $\alpha_{0,i}$ with respect to the horizontal; its members

have length $L_{0,i}$ corresponding to the length of the longest self-equilibrated configuration, and an axial stiffness k_i that then varies upon deformation. An external load P is applied at the apex, which is free to move horizontally and vertically by υ_h and υ_v, respectively. More generically, further below, we refer to υ_p as to the displacement of the apex in the direction of the applied load.

2.3 Analysis of the Structural Assemblies

Two approaches are employed for the analysis of the structural assemblies. First, energy landscapes are used to represent and characterize the behavior of the compliant mechanism over its work space. Next, a path following method is applied to obtain the potential load paths for specific load cases.

2.3.1 Strain Energy Landscapes

Strain energy landscapes are an effective way to identify stable configurations of the structure at either global or local minima of the strain energy across the work space [23]. For this particular configuration of the assembly of double-helices (Fig. 4), where their free ends are connected to a single moving point (the apex), the total strain energy is uniquely determined by the position of this end effector, and is the sum of the strain energy of the constituent helical members given by Eq. (1). The strain energy landscapes provide a means to qualitatively compare the structural response of the truss structures.

2.3.2 Path-following Method

Previous studies on the behavior of the *von Mises* truss suggest that the structure undergoes a snap-through when loaded beyond a critical value with a vertical force at the apex [24,25]. As the double-helices are expected to introduce further nonlinearities, an iterative path-following algorithm is required to determine the load-displacement response of the structural assemblies. The arc-length method is an efficient method to solve nonlinear systems and capture behaviors like snap-through and snap-back including the areas of instability [26,27]. Specifically, we use the modified-Riks method developed by Crisfield [28]. Additionally, bifurcations and limit points are detected by investigating the eigenvalues of the system's tangential stiffness matrix. A perturbation based on the respective eigenvectors is then applied to the solution at the bifurcation points for the computation of the branching paths [29,30]. The stability of an equilibrium branch is characterized by the eigenvalues, with negative eigenvalues indicating instability. Combined, the path-following method and the stability analysis enable the load-displacement response of the structural assemblies to be characterized fully.

3. Results and Discussions

The results presented herein focus on the analysis of the simplest geometry for the structural assembly of double-helices, *i.e.* the modified *von Mises* truss as depicted in Fig. 4. The aim of this work is to highlight the richness of structural response available by studying the potential (strain) energy landscapes of the assembly and exploring load paths under various load conditions and for a variety of potential combinations of double-helices.

3.1 Initial Results

In the initial analyses all double-helices have the following geometric parameters: $L = 95$ mm, $R = 15$ mm, $R_i = 30$ mm, $W = 5$ mm. Two geometric configurations are considered: a shallow ($\alpha_{0,1} = 35°$) and a steep ($\alpha_{0,1} = 70°$) truss. Three composite lay-ups are chosen from Fig. 3 to represent the three types of curve in the graph and explore the ensuing responses of the structural assemblies: a unidirectional (UD) lay-up ($[0_5]$); a symmetric lay-up ($[45_2/0/45_2]$); and an antisymmetric lay-up ($[45_2/0/-45_2]$). These truss and double-helix configurations are selected to illustrate representative obtainable properties. The strain energy landscapes for different truss configurations are presented in Fig. 5, allowing their stability characteristics to be explored; valleys correspond to stable equilibria, whereas peaks and saddle points denote unstable equilibria. Stable and unstable internal equilibria are labelled with Arabic numbers (1–5) and Roman letters (A–H, J, K and M), respectively. Latin numerals (I–IV) are used for stable boundary equilibrium positions, where at least one of the two helices is fully extended. For shallow trusses, the UD and symmetric lay-ups feature bistability, with stable states at the initial position and at a vertical displacement $2H_0$ (points 1 and 2 in Fig. 5a, b). For double-helices of antisymmetric lay-up, the assembly displays only unstable interior equilibria (points G, H and M in Fig. 5c), but four stable boundary equilibria can be observed (points I–IV in Fig. 5c). For steep trusses, the structure can exhibit: i) bistability, for a $[0_5]$ lay-up (points 1 and 2 in Fig. 5d); ii) quadristability, when double-helices of a symmetric lay-up are combined (points 1–4 in Fig. 5e); iii) pentastability, in

case of an antisymmetric lay-up, with a single interior stable point, when the double-helices are collinear with a zero horizontal displacement (point 5 in Fig. 5f), and an additional four boundary equilibria (points I–IV in Fig. 5f).
The force-displacement response for a *vertical* load at the apex is presented in Fig. 6. The corresponding positions of the apex are superimposed on the strain energy plots in Fig. 5 (red markers). For most cases, a bifurcation of the equilibrium path is present, resulting in both horizontal and vertical displacements of the apex. Interestingly, the bifurcated branches enable the mechanism to deform to all the possible internal equilibrium configurations identified on the strain energy landscape just by applying a vertical load at the apex. For shallow trusses with a $[0_5]$ lay-up or an antisymmetric one, where no bifurcation of the equilibrium path occurs, all internal equilibrium configurations are also traversed.

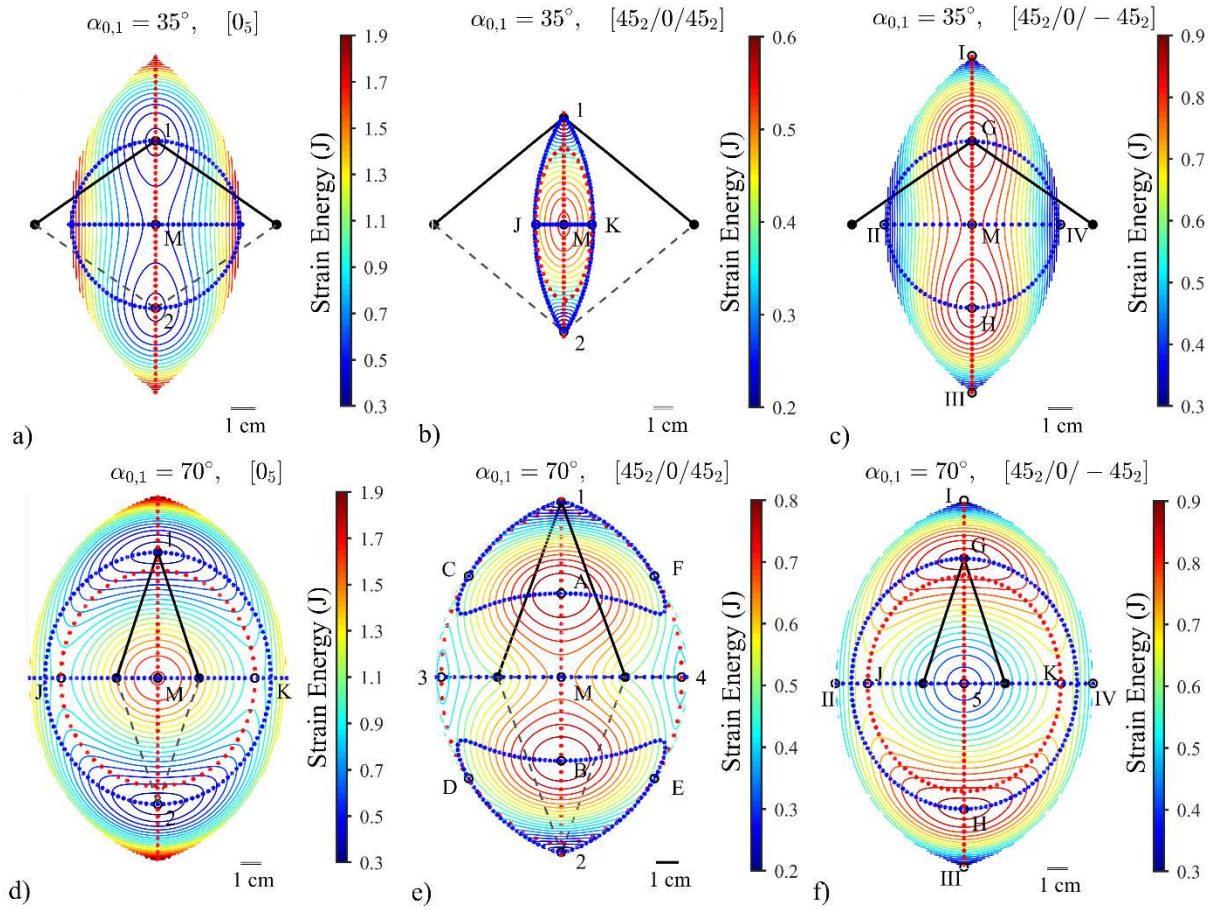

Figure 5: Strain energy landscapes for a compliant mechanism of identical double-helices assembled in a truss-like configuration. Results are for initial truss angles $\alpha_{0,1} = 35°$ and $\alpha_{0,1} = 70°$, with composite strips of $[0_5]$, $[45_2/0/45_2]$ and $[45_2/0/-45_2]$ lay-ups. The initial truss configurations are indicated with black lines. Points labelled 1–5 denote stable equilibria, while points A–H, J, K and M identify positions of unstable equilibrium; points I–IV denote stable boundary equilibria. The positions of the truss apex under an applied vertical load ($P_h = 0$) and/or horizontal load ($P_v = 0$) are superimposed on the landscapes: red points indicate the equilibrium paths of the apex under the application of a vertical load; blue points indicate the equilibrium paths of the apex under the application of a horizontal load.

The force-displacement response of the structure under a *horizontal* load at the apex is depicted in Fig. 7. The corresponding positions of the apex are superimposed on the strain energy plots in Fig. 5 (blue markers). A bifurcation of the equilibrium path occurs for all cases, except for double-helices of a symmetric lay-up assembled in a steep truss, where three disconnected equilibrium paths are observed (Fig. 5e). Similar to the case of a vertical applied load, all the internal equilibrium configurations can be traversed via the application of a horizontal load. Notable is the region of linear load-displacement response along the main equilibrium path despite the use of nonlinear elements. This response is accompanied by a circular displacement path of the apex, as illustrated in the respective strain energy plots (Fig. 5a, c, d, f). This region is a stable area of constant stiffness for the $[0_5]$ lay-up, but is unstable for double-helices of antisymmetric lay-up (Fig. 7). The use of double-helices with symmetric lay-up provokes non-linear behavior, particularly for a steep truss. Additionally, for this configuration, a jump in the load-displacement curve of one of the disconnected equilibrium paths is noticed

(Fig. 7b). The mechanics of this jump is explained in section 3.3. In all cases closed-loop deformation paths of the apex can be observed.

Figure 8 shows the response of the assembly of double-helices with symmetric lay-up in a shallow truss configuration under a *combined* loading ($P_h = P_v$). A more complex behavior is observed with the load-displacement curve forming an "S-shaped" curve. Although no bifurcation of the equilibrium path occurs, the mechanism nonetheless traverses all five equilibrium points. The structure also maintains its bistability as the energy minimum exists independent of the loading conditions.

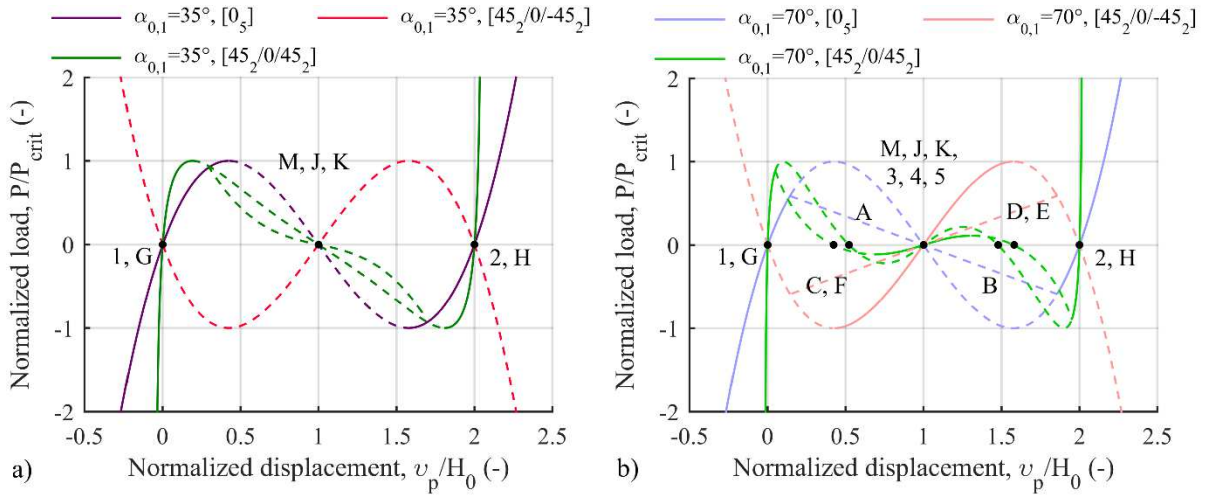

Figure 6: Load-displacement curves of the assembled structure of identical double-helices under the application of a vertical load at the apex. Results are for different initial truss angle a) $\alpha_{0,1} = 35°$ and b) $\alpha_{0,1} = 70°$ and of double-helices with varying lay-ups. Dashed line represents sections of instability; points 1–5 are stable equilibrium points. Points A–H, J, K and M are unstable equilibrium points. The load has been normalized with respect to the load value at the maximum peak (P_{crit}) in each case. The displacement has been normalized with respect to the initial height of the truss structure.

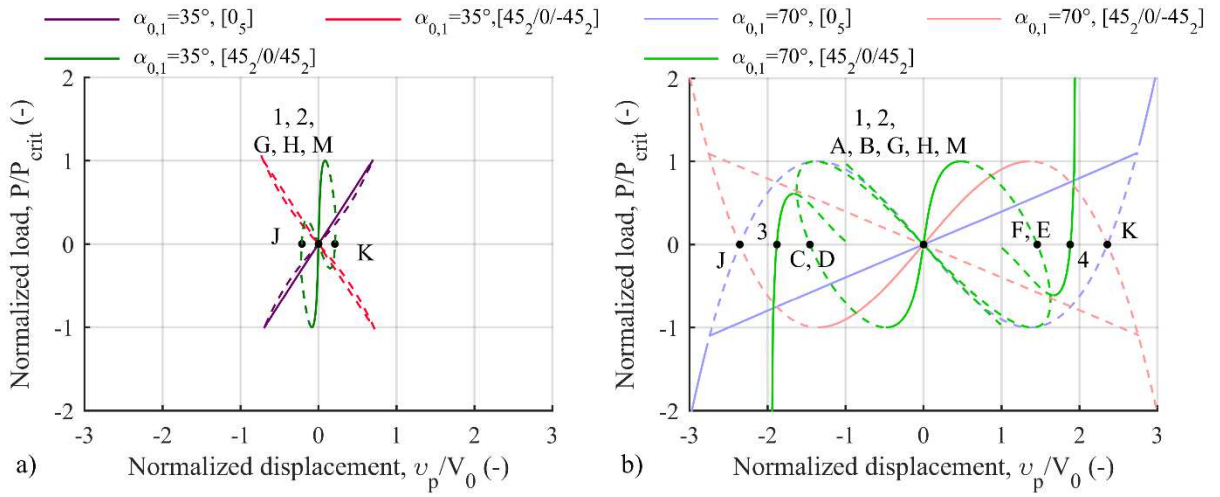

Figure 7: Load-displacement curves of the assembled structure of identical double-helices under the application of a horizontal load at the apex. Results are for different initial truss angle a) $\alpha_{0,1} = 35°$ and b) $\alpha_{0,1} = 70°$ and of double-helices with varying lay-ups. Dashed line represents sections of instability. Points 1 and 2 are stable equilibrium points; points A–H, J, K and M are unstable equilibrium points. The load has been normalized with respect to the load value at the maximum peak (P_{crit}) in each case. The displacement has been normalized with respect to the initial width of the truss structure.

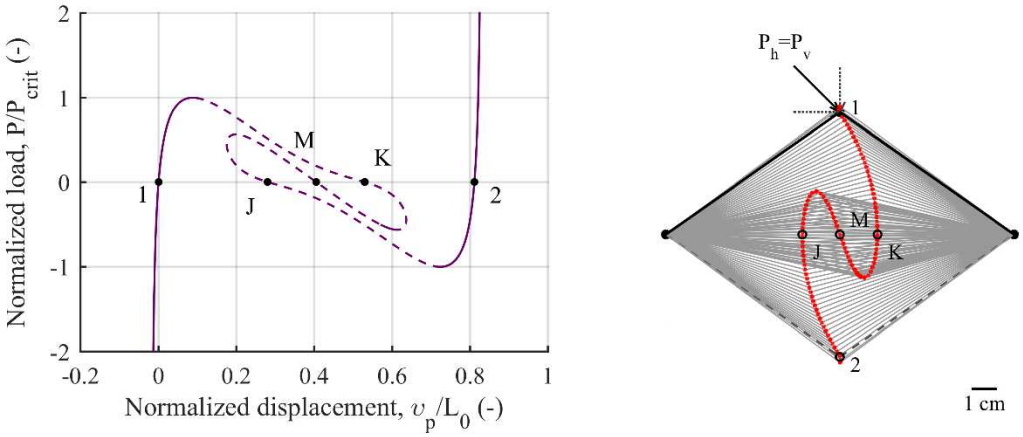

Figure 8: Load-displacement curve (left) and deformation (right) of the assembled structure (with initial angle $\alpha_{0,1} = 35°$) of two identical double-helices (with a [45₂/0/45₂] lay-up) under combined loading ($P_h = P_v$) at the apex. Points 1 and 2 are stable equilibrium points; points J, K and M are unstable equilibrium positions. Dashed lines (left) represents areas of instability. The load has been normalized with respect to the load value at the maximum peak (P_{crit}). The displacement has been normalized with respect to the initial length L_0.

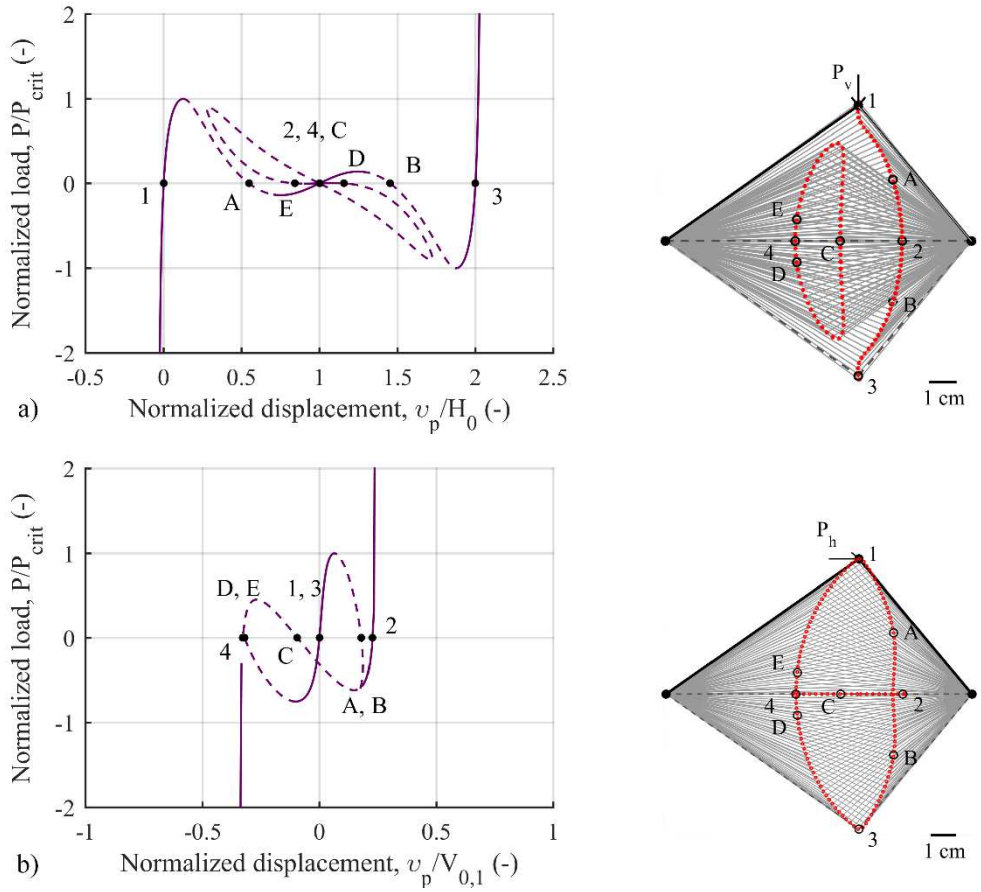

Figure 9: Load-displacement curves (left) and deformation (right) of the assembled structure of double-helices of different length under the application of a) a vertical load and b) a horizontal load at the apex. Points 1–4 are stable equilibrium points; points A–E are unstable equilibrium points. The truss has initial angle $\alpha_{0,1} = 35°$ and double-helices of [45₂/0/45₂] lay-up, and lengths $L_1 = 95$ mm, $L_2 = 71$ mm. Dashed lines (left) represent areas of instability. The load has been normalized with respect to the load value at the maximum peak (P_{crit}) for each case. The displacement has been normalized with respect to the initial height or width of the truss structure, respectively for vertical or horizontal loading.

Combining double-helices of different properties further expands the ability to tailor the force-displacement response of the structural assemblies. Illustratively, Fig. 9 shows the response of double-helices of identical symmetric lay-up $[45_2/0/45_2]$ but with different lengths L, combined in a shallow truss. It is noted that any symmetry present in previous cases in the assembled structure is lost. The assembled structure experiences quadristability. Under a vertical load, two disconnected equilibrium paths are identified, one of which forms a closed loop, while a horizontal load results in a bifurcation of the equilibrium path. In both loading conditions all possible equilibria, both stable and unstable, are accessed. Further investigation of asymmetric trusses is beyond the scope of this paper, and we focus on cases of using truss members of the same properties.

In the following sections the sensitivity of salient behaviors identified above—specifically, multistability and constant stiffness—to changes in design parameters of the structure is further explored.

3.2 Multistability

Two double-helices with a symmetric $[45_2/0/45_2]$ lay-up assembled into a steep truss with initial angle $\alpha_{0,1} = 70°$ exhibit four stable internal equilibrium configurations (see Fig. 5e). Multistable mechanisms have found use in applications such as switches, positioners, and reconfigurable structures [31]. The characteristics of multistability of the trusses are therefore of particular interest. Here, we explore the effect of linear springs, initial truss geometry, and lay-up of the composite strips, on the reference configuration. For comparison purposes, the values in the load-displacement graphs (Figs. 10–12) have been normalized with respect to a critical load—the maximum peak of the load-displacement curve—and the initial height of the truss structure.

Replacing the double-helices with linear springs results in the loss of quadristability, although a bifurcation of the equilibrium path is still present (see Fig. 10). While points 3 and 4 (Fig. 10a) are stable equilibrium positions for the case of double-helices, for linear springs these positions labelled as J and K become unstable. Points 3, 4, J and K refer to positions where the truss elements are collinear (Fig. 10b). For both linear springs and double-helices the axial forces have opposite sign, thus the system self-equilibrates. For the case with linear springs (points J and K in Fig. 10b) the equilibrium is unstable. Conversely, for the case with double-helices (points 3 and 4 in Fig. 10b), the two helices also have axial stiffnesses of opposite sign: the helix displaying negative axial force has negative stiffness. As a consequence, the helices tend to deform in opposite directions, which ultimately stabilizes the equilibrium state (Fig. 10c).

The initial geometry of the assembled structure significantly affects its multistable behavior. A shallow truss ($\alpha_{0,1} = 35°$) is bistable, while for higher initial truss angles, $\alpha_{0,1} = 45°$ or $\alpha_{0,1} = 70°$, the mechanism exhibits quadristability under the application of a vertical load (Fig. 11a). This behavior is closely linked to the characteristics of the double-helices themselves. In shallow trusses the two stable positions are the initial one and the one at a vertical displacement equal to $2H_0$ (points 1 and 2, respectively, in Fig. 11a), while points M, J and K are unstable equilibria. Positions J and K on the bifurcation path, which occur when the double-helices are horizontal, are noticed in steeper trusses too, but as stable equilibria (points 3 and 4 in Fig. 11a). In these stable equilibrium positions—where the helices are collinear—the double-helices have axial stiffness of opposite sign and the axial forces have either opposite sign (points 3 and 4 for $\alpha_{0,1} = 70°$ in Fig. 11b) or are both negative (points 3 and 4 for $\alpha_{0,1} = 45°$ in Fig. 11b). In either case, due to the different truss geometry, the helices pull against each other, thus stabilizing the equilibrium.

The lay-up of the composite strips of the double-helix can significantly affect the load-displacement behavior of the double-helix (Fig. 3). The reference structure consists of double-helices with a symmetric $[45_2/0/45_2]$ lay-up. In Fig. 12, we explore the behavior of the mechanism for varying ply angle β in symmetric lay-ups of the form $[\beta_2/0/\beta_2]$. For a ply angle $\beta = 0°$ the assembly is bistable, with both the initial configuration and the configuration at vertical displacement $2H_0$ being stable (points 1 and 2 in Fig. 12). Note that none of the equilibrium points encountered on the secondary path correspond to a stable state in this case. For a ply angle $\beta = 90°$ the double-helix load-displacement curve is similar to that of an antisymmetric lay-up (Fig. 3), thus the characteristics of the mechanism with $\beta = 90°$ or an antisymmetric lay-up are the same, with the structure exhibiting one internal stable equilibrium when the double-helices are collinear (point 5 in the main path, Fig. 12), plus four boundary equilibria (Fig. 5f). For all other ply angles, $0° < \beta < 90°$, the assembly is quadristable. For the relevant deformation of the truss structures the reader is referred to Fig. 5d-f.

Variations in the geometrical features of the double-helix result in minor differences in its load-displacement behavior (Appendix A.1) and thus have a limited effect on the multistability of the mechanism. Relevant graphs of load-displacement for different geometrical characteristics of the double-helices have been included in Appendix A.2.

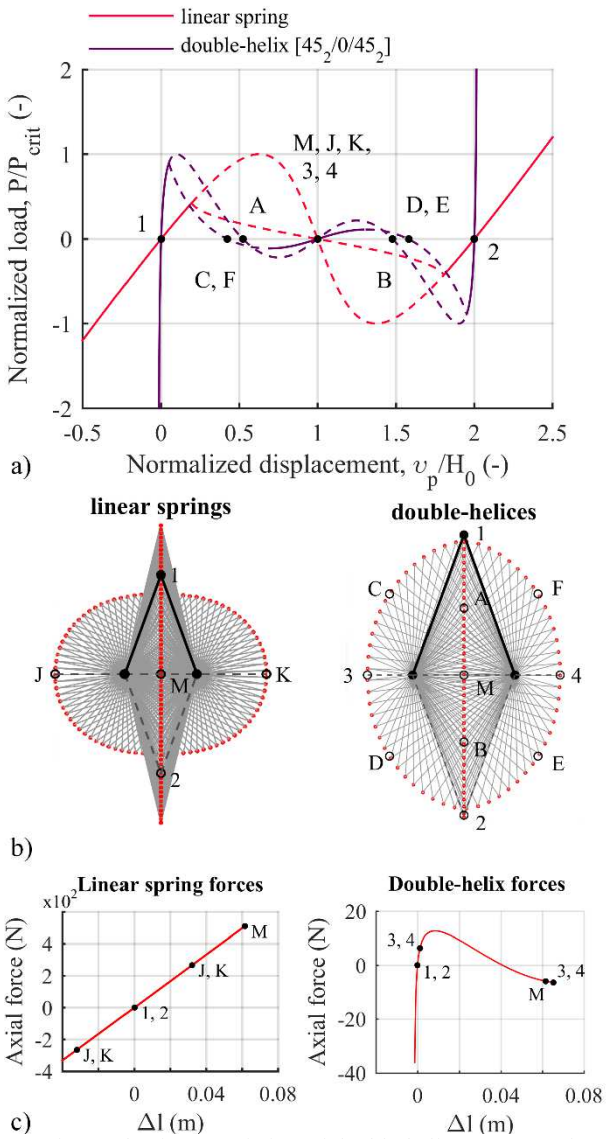

Figure 10: a) Load-displacement curve of a mechanism consisting of double-helices compared to one of linear springs under a vertical load at the apex. Initial truss angle $\alpha_{0,1} = 70°$ is used for both assemblies. Points 1–4 are stable equilibrium points; points A–F, J, K and M are unstable equilibrium points. Dashed lines represent areas of instability. b) Deformation of the assembled structures. c) Axial force with respect to displacement of a linear spring (left) and of a double-helix (right).

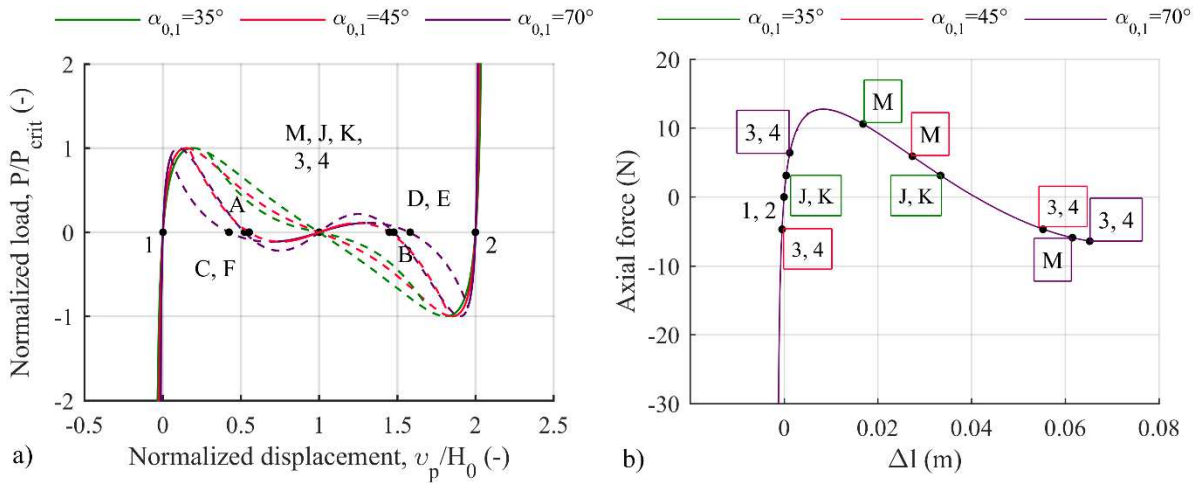

Figure 11: a) Load-displacement curves of a mechanism with different initial truss angles $\alpha_{0,1}$ consisting of double-helices of [45_2/0/45_2] lay-up, under the application of a vertical load at the apex. Points 1–4 are stable equilibrium points. Points A–F, J, K and M are unstable equilibrium points. Dashed lines represent areas of instability. b) Axial forces of double-helices at selected equilibrium points for the different initial truss angles.

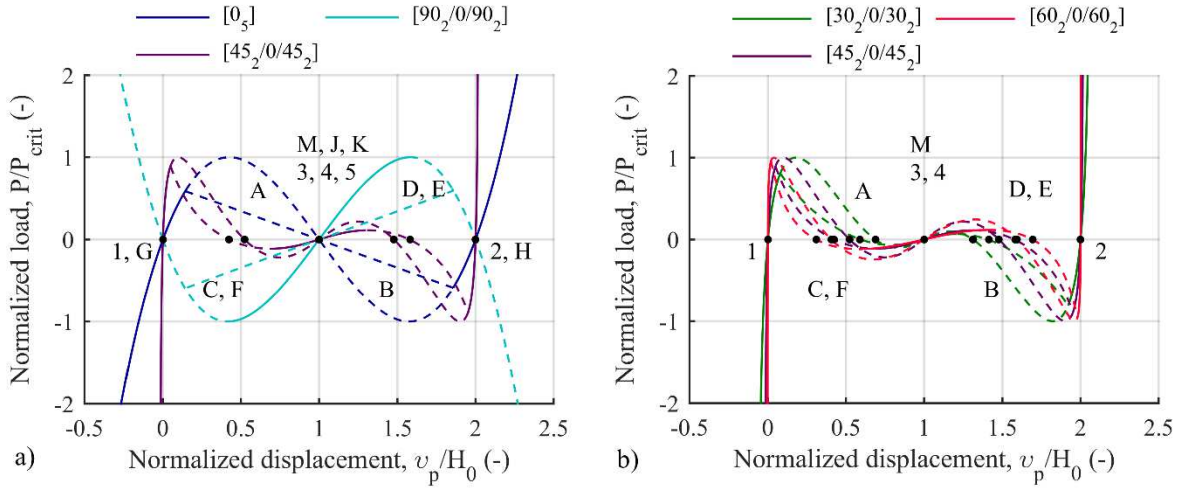

Figure 12: Load-displacement curves of the assembled structure of identical double-helices for different symmetric lay-ups of the form of [β_2/0/β_2] for a) β = 0°, 45°, 90° and b) β = 30°, 45°, 60° under the application of a vertical load at the apex. Points 1, 2 and 5 are stable equilibrium points on the main paths; points 3 and 4 on the bifurcation paths. Points A, M, B, G and H are unstable equilibrium points on the main paths; points C–F, J and K on the bifurcation paths. Dashed lines represent areas of instability.

3.3 Constant Stiffness

Another interesting behavior from the initial results is the development of a mechanism of constant stiffness while undergoing large deformations under a horizontal load at the apex. The mechanism consisting of double-helices of [0_5] lay-up, L = 95 mm, R = 15 mm, R_i = 30 mm and W = 5 mm, at an initial truss angle $\alpha_{0,1}$ = 70°, exhibits a stable main equilibrium path with constant stiffness, and is used as the reference mechanism for this feature. To investigate the reasons producing constant stiffness, Fig. 13 presents a comparison to the case of a truss with linear springs instead of double-helices. In both cases bifurcation of the main equilibrium path is present. However, our focus here is on the behavior of the main equilibrium path. The mechanism consisting of linear springs does not exhibit constant stiffness and its deformation follows an ellipsoidal path under the application of a horizontal load at the apex, while the reference mechanism of double-helices presents a linear load-displacement response (Fig. 13a)—verified by the expression of the best fit curve ($y = 0.4001x$, SE = 0.003)—and a circular deformation path. The circular path has radius $r = H_0$ and is centered at the midpoint between the supports (Fig. 13b). Trusses of different initial geometry $\alpha_{0,1}$ all exhibit a linear load-displacement response corresponding to the main equilibrium path, while the bifurcated branch is nonlinear (Fig. 14). A shallow truss presents a higher stiffness to a horizontal

load at the apex. In all cases the main deformation path of the apex is circular, with a horizontal bifurcation path across the diameter when the apex is level with the supports (blue markers in Fig. 5a, d).
Changes in the lay-up of the strips of the double-helix have a more significant impact on the behavior of the compliant mechanism (Fig. 15). Specifically, for $\beta = 0°$ the mechanism exhibits a linear load-displacement response of the main equilibrium path and bifurcates to a path with a nonlinear response. The main path with constant stiffness is stable, compared to the bifurcated branch which is generally unstable. The mechanism exhibits a similar behavior for a $[90_2/0/90_2]$ lay-up, but in this case the path with constant stiffness characteristics is unstable. For all other ply angles $0° < \beta < 90°$, a nonlinear load-displacement response is observed, and no bifurcation of the equilibrium path occurs. Instead, three independent equilibrium paths are identified—two mirrored closed-loop paths with identical load-displacement curves, and a horizontal path along the horizontal diameter, *i.e.* when the apex is level to the supports. This equilibrium branch presents a jump in the corresponding load-displacement curve at the positions where the apex traverses the supports ($v_h = \pm V_0$). At these positions, the fully coiled helix turns around the support and switches direction uncoiling out and away from the hinge point. In this scenario the helix reaction force too switches direction, which justifies the sudden jump in the equilibrium manifold. Indicatively, the reader can refer to Fig. 5e, which depicts the deformation of the mechanism with double-helices of a $[45_2/0/45_2]$ lay-up (blue markers). In all cases closed-loop-deformation paths can be observed.
Less significant is the influence of the double-helix geometry on the behavior of the assembled structure. The relevant load-displacement curves can be found in the Appendix A.3.

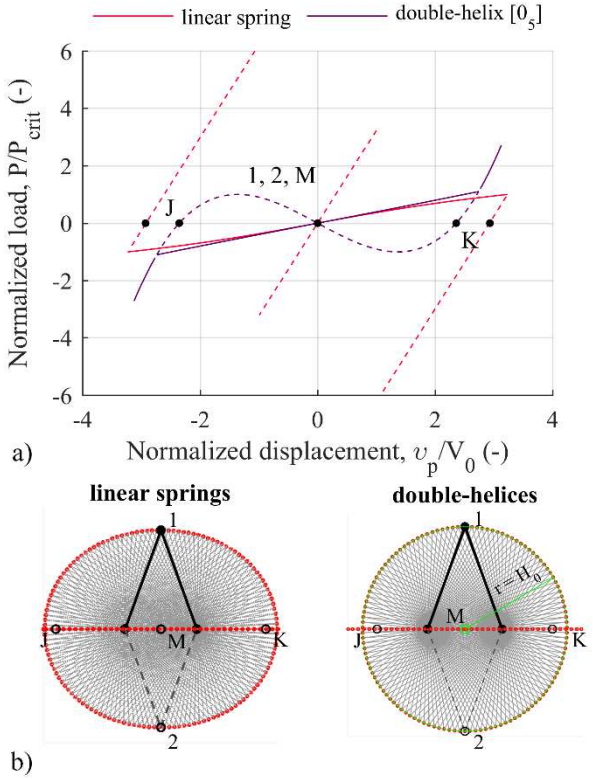

Figure 13: a) Load-displacement curve of a mechanism consisting of double-helices compared to one of linear springs under a horizontal load at the apex. Initial truss angle $\alpha_{0,1} = 70°$ is used for both assemblies. Dashed lines represent areas of instability. b) Deformation of the assembled structures of linear springs (left) and of double-helices (right). Points 1 and 2 are stable equilibrium positions; points J, K and M are unstable equilibrium positions.

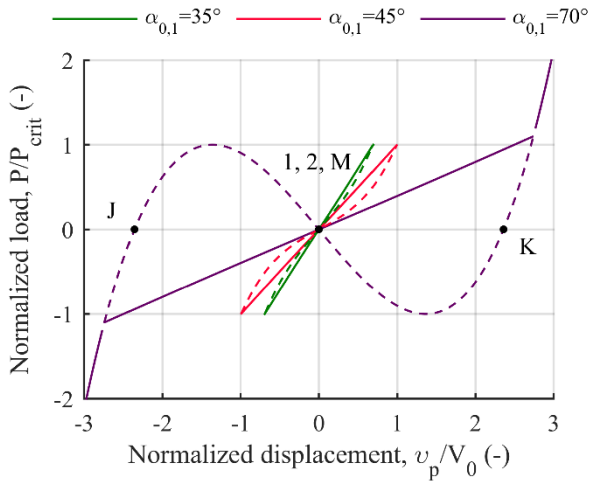

Figure 14: Load-displacement curves of a mechanism of different initial truss angles $\alpha_{0,1}$ consisting of double-helices of $[0_5]$ lay-up, under the application of a horizontal load at the apex. Points 1 and 2 are stable equilibrium points; points J, K and M are unstable equilibrium points. Dashed lines represent areas of instability.

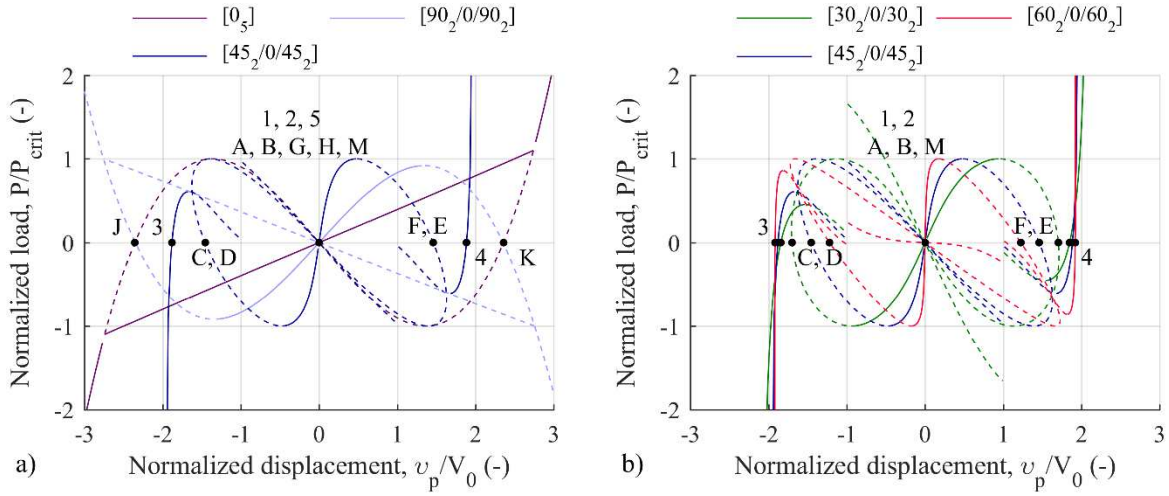

Figure 15: Load-displacement curves of the assembled structure of identical double-helices for different symmetric lay-ups of the form of $[\beta_2/0/\beta_2]$ for a) $\beta = 0°$, 45°, 90° and b) $\beta = 30°$, 45°, 60° under the application of a horizontal load at the apex. Points 1–5 are stable equilibrium points; points A, C, F–H, J, K and M are unstable equilibrium positions. Dashed lines represent areas of instability.

4. Experimental Results and Discussion

This section presents initial test results to validate the analytical model and assess the feasibility of the proposed mechanism. The preliminary results are part of a broader experimental campaign that constitutes future work. A truss prototype was manufactured and tested under application of a vertical load at the apex. For the manufacture of the double-helices we followed the process described in [15]. Figure 16 shows the experimental set-up. The double-helices are attached to a base frame on one end and to a rod on the opposite end, forming the apex of the truss mechanism. The rod is attached to the crosshead of a universal testing machine and is free to move vertically but restricted to move horizontally. To achieve configurations where the apex experiences both horizontal and vertical displacements, the base of the truss mechanism is designed to have unconstrained horizontal movement by rolling along a lower frame fixed to the test machine; similarly to the solution in [32]. The result is a test arrangement which is statically equivalent to the system depicted in Fig. 4.

An AGS-X Series Shimadzu test machine with 1 kN load cell and a precision of 1% was used to perform the test and apply a vertical load on the fixture. A displacement-control loading was employed for the tests at a rate of 0.5 mm/sec. Both vertical load and displacement were recorded using the Trapezium X software of the Shimadzu machine. To capture the horizontal displacement of the base frame, and thus of the truss apex, an Imetrum Video Gauge camera system, with 17 fps frame rate and a 1392 x 1040 pixel camera with a 25 mm focal length lens, was used.

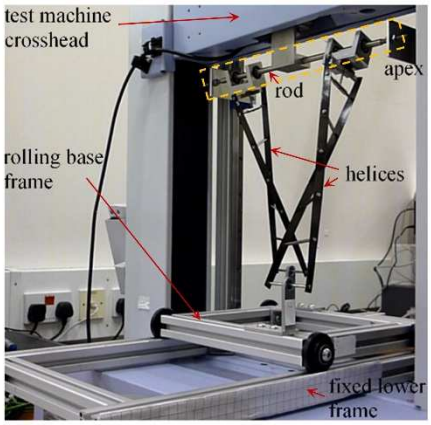

Figure 16: Experimental set-up.

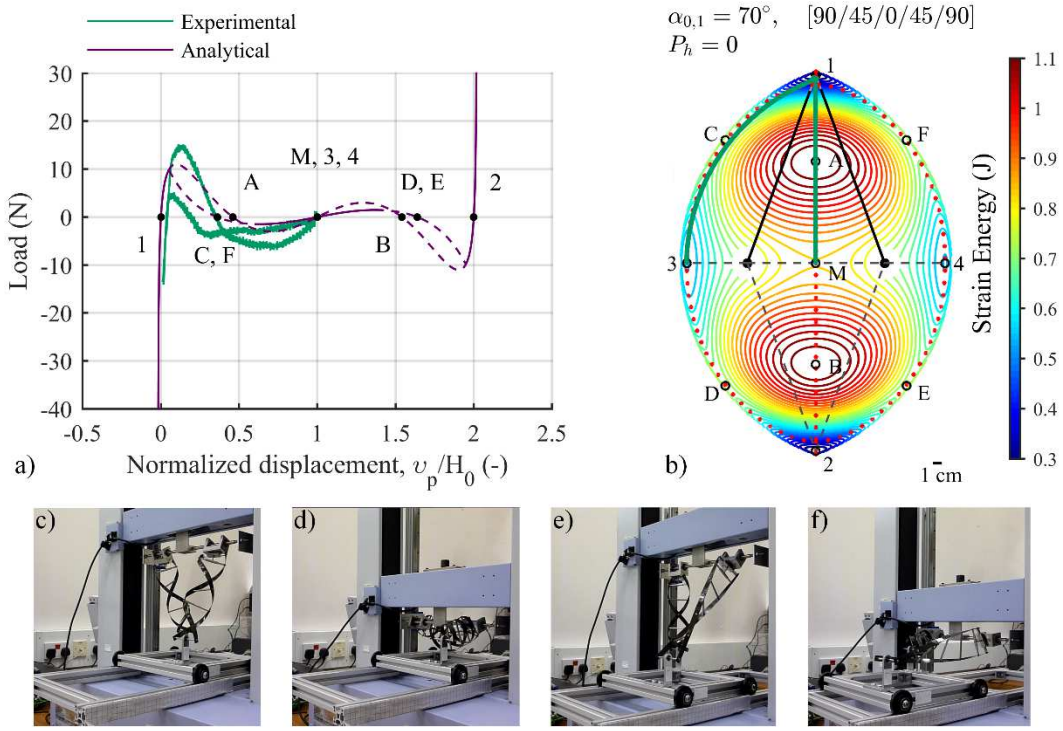

Figure 17: a) Load-displacement curves under the application of a vertical load at the apex of the truss of double-helices. Dashed lines represent areas of instability for the analytical data. The truss has initial angle $\alpha_{0,1} = 70°$ and double-helices of [90/45/0/45/90] lay-up, with dimensions $L = 292$ mm, $R = 30$ mm, $R_i = 60$ mm, $W = 10$ mm. b) Corresponding strain energy landscape with the positions of the truss apex under an applied vertical load ($P_h = 0$) at the end effector superimposed; red markers are used for the analytical and green markers for the experimental data. Points 1–4 are stable equilibrium points. Points A–F and M are unstable equilibrium points. c-f) Different configurations of the prototype during testing: c) a configuration along the main path between points 1 and A with both helices twisted equally; d) a configuration close to point M, with the helices collinear and twisted equally; e) a configuration on the bifurcation path between points 1 and C, with the helices twisted to different extent; f) a configuration close to point 3, with the helices collinear but one in a slightly twisted and the other in a coiled configuration.

The experimental results for a truss of double-helices with symmetric lay-up assembled in a steep configuration are included in Fig. 17 and compared to the corresponding analytical results. The double-helices have dimensions $L = 292$ mm, $R = 30$ mm, $R_i = 60$ mm, $W = 10$ mm, and a [90/45/0/45/90] lay-up. The analytical results are updated, taking into consideration also the length required for the end fittings of the helices. For simplicity, owing to the vertical and horizontal symmetry of the mechanism, the test of the prototype is performed for a quarter of the design space. The load-displacement curves as predicted by the analytical model and the experimental data are in good qualitative agreement. Some differences

in the actual values are observed that can be attributed to a variety of reasons, including: i) friction, which is unaccounted for in the model, both between the spokes and the composite helical strips and at all other joints in the fixture; ii) nonuniform deformation of the helix noticed during the test, with the pitch varying across the helix length which was not observed in previous work by Lachenal *et al.* [15] and is presumably dependent on the length-to-radius ratio of the helices; iii) the spokes of the helices touching during coiling/uncoiling as a result of the nonuniform helix deformation, evidenced by slight kinks in the load-displacement curves; iv) any imperfections during manufacturing of the helices.

5. Conclusions

A truss-like mechanism consisting of morphing elements has been introduced. The morphing elements consist of composite strips in a double-helix architecture and are capable of large axial deformations. These helical structures exhibit highly tailorable nonlinear stiffness characteristics, thus enabling the ensuing mechanism to feature a variety of structural responses. This paper explored the rich design space of such mechanism; by tailoring the inherent properties of its elements—and subsequently its architecture—access to a wide design space is opened up.

Two analysis methods have been employed to explore the properties of the structural assemblies. Strain energy landscapes are used to study the stability characteristics of the compliant mechanism qualitatively across its work space and to identify equilibrium configurations. To investigate the response to specific loads, a path following method with bifurcation tracking is employed to capture the full nonlinear response. Combined, these methods provide full insight into the mechanical properties of the compliant mechanisms.

Results herein focus on the simplest possible geometry, an assembly of two identical double-helices connected with pinned joints forming a truss-like structure. A variety of different behaviors has been observed through the energy landscapes, illustrating the rich design space. Quadristable behavior is obtained for steep trusses and symmetric composite lay-ups of the form $[\beta_2/0/\beta_2]$, with $0° < \beta < 90°$. For $\beta = 0°$ and $\beta = 90°$, the mechanism becomes bistable and pentastable, respectively. The mechanism transitions from quadristable to bistable for decreasing initial truss angles. Under the application of a vertical load at the apex, the equilibrium path bifurcates, enabling access to all internal equilibrium configurations. Under the application of a horizontal load at the apex, the mechanism demonstrates a stable region of constant stiffness for $\beta = 0°$, regardless of the initial truss angle, with the deformation path forming a circle. Again, bifurcations of the equilibrium path lead to connecting all internal equilibria. The type of structural behavior is found to depend primarily on the lay-up of the strips of the double-helices and the initial geometry of the structural assembly. The geometrical characteristics of the double-helices have limited effect on the behavior of the mechanism, thus making the concept scalable.

The study in this paper has focused on the numerical analysis of the structural assemblies of double-helices with the simplest possible geometry and with helices limited to pitches θ in the range $[0°, 90°]$. A prototype of the proposed mechanism was manufactured and tested by applying a vertical load at the apex to validate the analytical predictions. Future work will involve the development of further prototypes, recognizing the challenges that might exist in manufacturing the proposed mechanisms. At the same time, this work can be extended to exploring the behavior of mechanisms of more complex geometries, and/or taking advantage of the ability of the helical elements to deform to configurations with $\theta \in [0°, -90°]$, which leads to the development of different responses that can be used as the basis for reconfiguration of the mechanism. Additionally, a refinement to the prototype design and manufacture process would be required.

The rich mechanical response of this mechanism, with its ability to undergo large deformations maintaining a load-carrying capability, its multistable characteristics and highly tailorable nonlinearities, along with its potential reconfigurable behavior, could be promising for a wide spectrum of applications from positioners, actuators and energy harvesters to rehabilitation devices, deployable structures and vibration isolators, where such features are desirable.

Acknowledgments

CA is supported by the Engineering and Physical Sciences Research Council through the EPSRC Centre for Doctoral Training in Advanced Composites for Innovation and Science [grant number EP/L016028/1]. AP is supported through the EPSRC Fellowship titled *Structural Efficiency and Multi-Functionality of Well-Behaved Nonlinear Composite Structures* [grant number EP/M013170/1].

Data Statement

All data required to reproduce the figures in this paper are available at the data repository of the University of Bristol via the URL: https://doi.org/10.5523/bris.rb2p7tvx0xz2b2ielej67r9c

Appendix

A.1 Force-Displacement Response of Double-Helix Structures

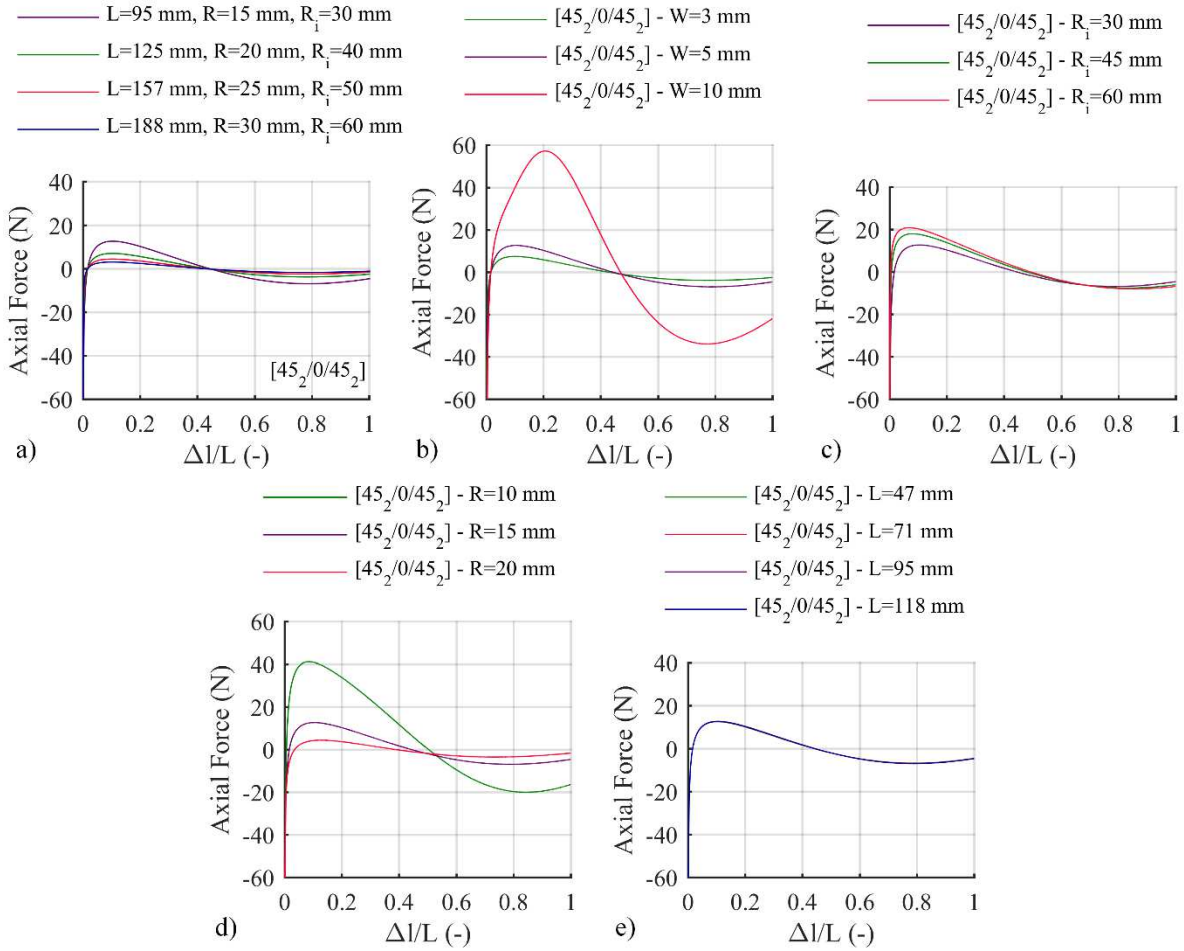

Figure 18: Load-displacement curves of double-helices: a) for different dimensions L, R and R_i, keeping a constant ratio $R_i/R = 2$ and $L \approx 2\pi R$, lay-up [45₂/0/45₂], $W = 5$ mm; b) for different widths W, lay-up [45₂/0/45₂], $L = 95$ mm, $R = 15$ mm, $R_i = 30$ mm; c) for different initial curvatures of the strips R_i, lay-up [45₂/0/45₂], $L = 95$ mm, $R = 15$ mm, $W = 5$ mm; d) for different radius R, lay-up [45₂/0/45₂], $L = 95$ mm, $R_i = 30$ mm, $W = 5$ mm; e) for different lengths L, lay-up [45₂/0/45₂], $R = 15$ mm, $R_i = 30$ mm, $W = 5$ mm. The displacement Δl is normalized to the length L of the strips in each case for comparison purposes, with $\Delta l/L = 0$ representing the fully-extended and $\Delta l/L = 1$ its fully coiled configuration.

A.2 Influence of Double-Helix Geometrical Features on Multistability

Variations in the width W of the strips, the radius R and the initial curvature of the strips R_i result in different load-displacement curves for the double-helices (Fig. 18). The influence of these parameters on the multistable behavior of the mechanism under an applied vertical load at the apex is explored in Fig. 19. The mechanism remains quadristable, although the stiffness of the structure will vary. Changing the length L of the double-helix has no effect on the double-helix response (Fig. 18f), so an investigation of this parameter on the response of the assembled structure is omitted. The ability of scaling up the structure is also explored. For this purpose, double-helices of different dimensions L, R, R_i but with constant ratios $R_i/R = 2$ and $L/R \approx 2\pi$ have been used. The load-displacement behavior of such double-helices is included in Fig. 18b and the response of an assembled structure of these helices is presented in Fig. 19a. The load-displacement curves of the different mechanisms are identical, meaning that the structure can be scaled up or down while maintaining the quadristable behavior.

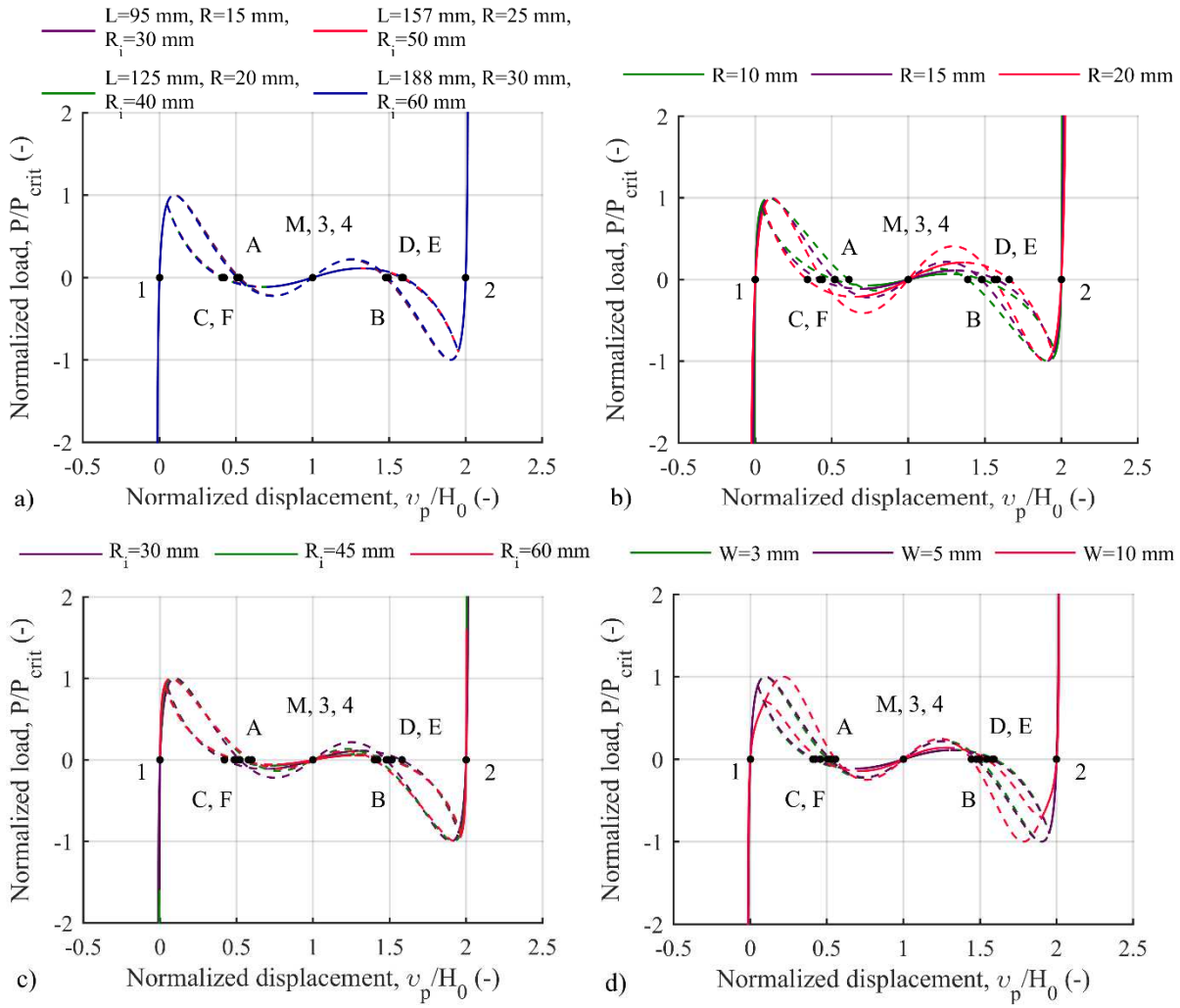

Figure 19: Load-displacement curves of the assembled structure of identical double-helices under the application of a vertical load at the apex, with different a) dimensions L, R and R_i, keeping a constant ratio $R_i/R = 2$ and $L \approx 2\pi R$, lay-up $[45_2/0/45_2]$, $W = 5$ mm; b) radius R, lay-up $[45_2/0/45_2]$, $L = 95$ mm, $R_i = 30$ mm, $W = 5$ mm; c) initial curvatures of the strips R_i, lay-up $[45_2/0/45_2]$, $L = 95$ mm, $R = 15$ mm, $W = 5$ mm; d) widths W, lay-up $[45_2/0/45_2]$, $L = 95$ mm, $R = 15$ mm, $R_i = 30$ mm. Points 1 and 2 are stable equilibrium points on the main path; points 3 and 4 on the bifurcation path. Points A, M and B are unstable equilibrium points on the main path; points C–F on the bifurcation path. Dashed lines represent areas of instability.

A.3 Influence of Double-Helix Geometrical Features on Constant Stiffness

The impact of varying the double-helix geometry on its response to a horizontal load applied at the apex is explored in Fig. 20. Mechanisms of different dimensions L, R, R_i but with constant ratios $R_i/R = 2$ and $L/R \approx 2\pi$ present no influence in the response with the load-displacement curves matching each other, giving the ability of scaling the mechanism to the required dimensions for an application (Fig. 20a). Varying the radius R or the initial curvature of the strips of the double-helices consisting the mechanism affect the mechanism's work space. Although the load-displacement curves coincide for most of the work space, for small values of the radius R and/or higher values of the R_i there are limitations to the maximum horizontal displacement of the mechanism thus in these cases the load-displacement curve does not have a bifurcated branch, instead it consists of two independent load paths (Fig. 20b, c). Changes in the width W of the strips of the double-helices has no significant influence on the response of the mechanism with the load-displacement curves being identical with a slight deviation being observed in the case of wider strips towards the maximum horizontal displacement.

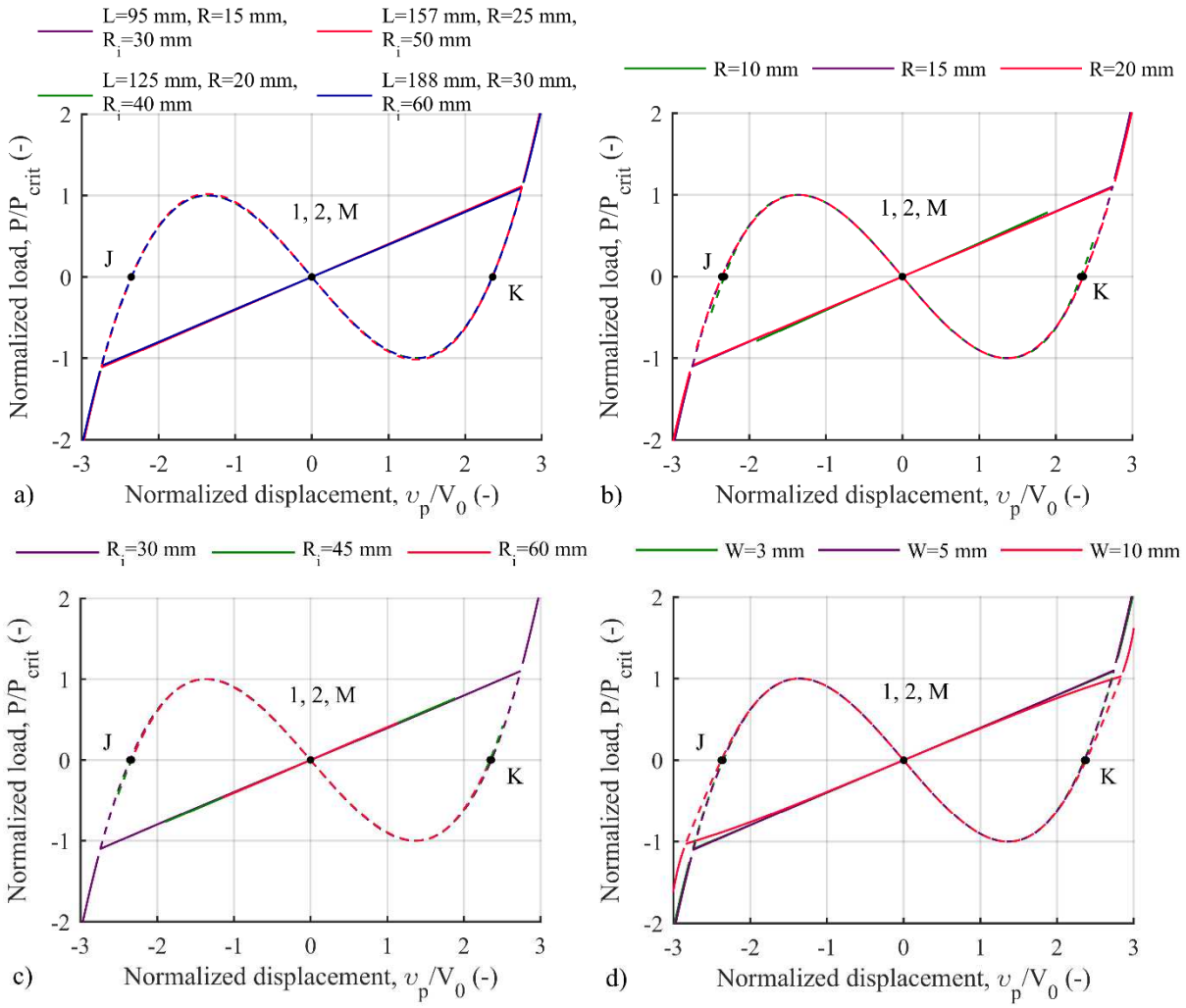

Figure 20: Load-displacement curves of the assembled structure of identical double-helices under the application of a horizontal load at the apex with different a) dimensions L, R and R_i, keeping a constant ratio $R_i/R = 2$ and $L \approx 2\pi R$, lay-up $[0_5]$, $W = 5$ mm; b) radius R, lay-up $[0_5]$, $L = 95$ mm, $R_i = 30$ mm, $W = 5$ mm; c) initial curvatures of the strips R_i, lay-up $[0_5]$, $L = 95$ mm, $R = 15$ mm, $W = 5$ mm; d) widths W, lay-up $[0_5]$, $L = 95$ mm, $R = 15$ mm, $R_i = 30$ mm. Points 1 and 2 are stable equilibrium points; points J, K and M are unstable equilibrium points. Dashed lines represent areas of instability.

References

[1] Hao, G., Yu, J., and Li, H., 2016, "A brief review on nonlinear modelling methods and applications of compliant mechanisms," Front. Mech. Eng., 11(2), pp. 119-128. DOI: 10.1007/s11465-016-0387-9

[2] Kim, C. J., Kota, S., and Moon, Y.-M., 2006, "An instant center approach toward the conceptual design of compliant mechanisms," ASME J Mech. Design, 128(3), pp. 542-550. DOI:10.1115/1.2181992

[3] Hu, Y. H., Lin, K. H., Chang, S. C., and Chang, M., 2008, "Design of a compliant micromechanism for optical-fiber alignment," Key Eng. Mat., 381-382, pp. 141-144. DOI: 10.4028/www.scientific.net/KEM.381-382.141

[4] Sung, E., Slocum, A. H., Ma, R., Bean, J. F., and Culpepper, M. L., 2011, "Design of an ankle rehabilitation device using compliant mechanisms," ASME J Med. Device, 5(1), pp. 011001-7. DOI: 10.1115/1.4002901

[5] Wilcox, D. L., and Howell, L. L., 2005, "Fully compliant tensural bistable micromechanisms (FTBM)," IEEE J Microelectromech. Syst., 14(6), pp. 1223-1235. DOI: 10.1109/JMEMS.2005.859089

[6] Aten, Q. T., Jensen, B. D., Burnett, S. H., and Howell, L. L., 2014, "A self-reconfiguring metamorphic nanoinjector for injection into mouse zygotes," Rev. Sci. Instrum., 85(5), pp. 055005. DOI: 10.1063/1.4872077

[7] Nelson, T. G., Lang, R. J., Pehrson, N. A., Magleby, S. P., and Howell, L. L., 2016, "Facilitating deployable mechanisms and structures via developable lamina emergent arrays," ASME J Mech. Robot., 8(3), pp. 031006. DOI: 10.1115/1.4031901

[8] Fowler, R. M., Howell, L. L., and Magleby, S. P., 2011, "Compliant space mechanisms: A new frontier for compliant mechanisms," Mech. Sci., 2(2), pp. 205-215. DOI: 10.5194/ms-2-205-2011

[9] Pellegrini, S. P., Tolou, N., Schenk, M., and Herder, J. L., 2013, "Bistable vibration energy harvesters: A review," J Intel. Mat. Syst. Str., 24(11), pp. 1303-1312. DOI: 10.1177/1045389X12444940

[10] Shaw, A. D., Neild, S. A., Wagg D. J., Weaver, P. M., and Carrella, A., 2013, "A nonlinear spring mechanism incorporating a bistable composite plate for vibration isolation," J Sound. Vib., 332(24), pp. 6265-6275. DOI: 10.1016/j.jsv.2013.07.016

[11] Rivlin, B., and Elata, D., 2012, "Design of nonlinear springs for attaining a linear response in gap-closing electrostatic actuators," Int. J Solids Struct., 49(26), pp. 3816-3822. DOI: 10.1016/j.ijsolstr.2012.08.014

[12] Torrealba, R. R., and Udelman, S.B., 2016, "Design of cam shape for maximum stiffness variability on a novel compliant actuator using differential evolution," Mech. Mach. Theory, 95, pp. 114-124. DOI: 10.1016/j.mechmachtheory.2015.09.002

[13] Trease, B. P., Moon, Y.-M., and Kota, S., 2005, "Design of large-displacement compliant joints," ASME J Mech. Design, 127(4), pp. 788-798. DOI: 101115/1.1900149

[14] Lachenal, X., Weaver, P. M., and Daynes, S., 2014 "Influence of transverse curvature on the stability of pre-stressed helical structures," Int. J Solids Struct., 51(13), pp. 2479-2490. DOI: 10.1016/j.ijsolstr.2014.03.014

[15] Lachenal, X., Weaver, P. M., and Daynes, S., 2012, "Multi-stable composite twisting structure for morphing applications," Proc. R Soc. A: Math. Phys. Eng. Sci., 468(2141), pp. 123051. DOI: 10.1098/rspa.2011.0631

[16] Fleck, N. A., Deshpande, V. S., and Ashby, M. F., 2010, "Micro-architectured materials: past, present and future," Proc. R Soc. A: Math. Phys. Eng. Sci., 466(2121), pp. 2495-2516. DOI: 10.1098/rspa.2010.0215

[17] Vigliotti, A., and Pasini, D., 2012, "Stiffness and strength of tridimensional periodic lattices," Comput. Methods Appl. Mech. Eng., 229-232, pp. 27-43. DOI: 10.1016/j.cma.2012.03.018

[18] Haghpanah, B., Salari-Sharif, L., Pourrajab, P., Hopkins, J., and Valdevit, L., 2016, "Multistable shape-reconfigurable architected materials," Adv. Mater., 28(36), pp. 7915-20. DOI: 10.1002/adma.201601650

[19] Cappello, L., Lachenal, X., Pirrera, A., Mattioni, F., Weaver, P. M., and Masia, L., 2014, "Design, characterization and stability test of a multistable composite compliant actuator for exoskeletons," *5th IEEE RAS/EMBS International Conference on Biomedical Robotics and Biomechatronics*, Sao Paulo, Brazil, August 12-15, 2014, pp. 1051-1056. DOI: 10.1109/BIOROB.2014.6913919

[20] Kollar, L. P., and Springer, G. S., 2003, *Mechanics of Composite Structures*, Cambridge University Press, Cambridge, UK. DOI: 10.1017/CBO9780511547140

[21] Giomi, L., and Mahadevan, L., 2011, "Multistability of free spontaneously-curved anisotropic strips," Proc. R Soc. A: Math. Phys. Eng. Sci., 468(2138), pp. 511-530. DOI: 10.1098/rspa.2011.0247

[22] Aza, C., Pirrera, A., Schenk, M., 2018, "Reconfigurable Trusses of Nonlinear Morphing Elements," *ASME International Design Engineering Technical Conferences and Computers and Information in Engineering Conference (IDETC/CIE2018)*, Quebec City, Quebec, Canada, August 26-29, 2018, Paper No. DETC2018-85911. DOI: 10.1115/DETC2018-85911

[23] Radaelli, G., Gallego, J. A., and Herder, J. L., 2011, "An energy approach to static balancing of systems with torsion stiffness," ASME J Mech. Design, 133(9), pp. 091006. DOI: 10.1115/1.4004704

[24] Bazant, Z. P., and Cedolin, L., 2010, *Stability of Structures: Elastic, Inelastic, Fracture and Damage Theories*, 3rd Ed, World Scientific Publishing. DOI: 10.1142/7828

[25] Galishnikova, V., Dunaiski, P., and Pahl, P. J., 2009, *Geometrically Nonlinear Analysis of Plane Trusses and Frames*, SUN PRESS. DOI: 10.18820/9781920109998

[26] Oh, Y. S., and Kota, S., 2009, "Synthesis of multistable equilibrium compliant mechanisms using combinations of bistable mechanisms," ASME J Mech. Design, 131(2), pp. 0210021-11. DOI: 10.1115/1.3013316

[27] Crisfield, M. A., 1981, "A fast incremental/iterative solution procedure that handles "snap-through"," Comput. Struct., 13(1-3), pp. 55-62. DOI: 10.1016/0045-7949(81)90108-5

[28] Reddy, J. N., 2015, *An Introduction to Nonlinear Finite Element Analysis: with applications to heat transfer, fluid mechanics, and solid mechanics*, 2nd Ed, Oxford University Press 2015. DOI: 10.1093/acprof:oso/9780199641758.001.0001

[29] Wagner, W., and Wriggers, P., 1988, "A simple method for the calculation of postcritical branches," Eng. Comput., 5(2), pp. 103-109. DOI: 10.1108/eb023727

[30] Wriggers, P., and Simo, J. C., 1990, "A general procedure for the direct computation of turning and bifurcation points," Int. J Numer. Meth. Eng., 30(1), pp. 155-176. DOI: 10.1002/nme.1620300110

[31] Chen, G., Aten, Q. T., Zirbel, S., Jensen, B. D., and Howell, L. L., 2010, "A tristable mechanism configuration employing orthogonal compliant mechanisms," ASME J Mech. Robot., 2(1), pp. 014501-014501-6. DOI: 10.1115/1.4000529

[32] Radaelli, G., and Herder, J. L. 2016, "A monolithic compliant large-range gravity balancer," Mech. Mach. Theory, 102, pp. 55-67. DOI: 10.1016/j.mechmachtheory.2016.03.015

Figure Caption List